Z. Phys. D 31, 85–93 (1994)

ZEITSCHRIFT
FÜR PHYSIK D

Producing and detecting very large clusters

U. Zimmermann, N. Malinowski*, U. Näher, S. Frank, T.P. Martin

Max-Planck-Institut für Festkörperforschung, Heisenbergstrasse 1, D-70569 Stuttgart, Germany (Fax: 0711-689-1010)

Received: 15 November 1993 / Final version: 5 February 1994

Abstract. The cluster source we use, a low pressure, rare gas condensation cell, is capable of producing clusters containing more than 45000 atoms or having masses exceeding 2 500000 amu. Details of this source and the dependence of the cluster size distribution on adjustable working parameters (oven temperature, inert gas pressure, inert gas type) are discussed in this report. Measurements of the mass-dependent velocity distributions of the clusters emitted by the source are presented and compared to a simple model calculation. The clusters are mass-analyzed with a time-of-flight mass spectrometer and detected by a multi-channel plate. The dependence of the detectability of large clusters on the acceleration voltage is investigated.

PACS: 36.40.+d; 07.75.+h; 07.77.+p

1. Introduction

One of the main peculiarities of clusters making their study so rewarding is the fact that these small aggregates of atoms no longer behave like a molecule nor do they yet show the properties of bulk material.

The transition from the molecule to the cluster has been and is being intensively studied [1]. There is, however, still a lack of understanding in the transition from cluster to bulk. Take, for example, the geometric structure of sodium or calcium clusters: even when containing thousands of atoms, they still have icosahedral or cuboctahedral structure, both not consistent with the bcc-structure of the bulk material [2–5]. To gain more insight into the transition to bulk, the study of larger clusters, preferably in the gas phase, has to be continued.

Our cluster source, a low pressure, rare gas condensation cell, can produce a cluster beam containing very large clusters, for example Na-clusters with more than 45000 atoms (1000000 amu) and Cs-clusters with masses of up to 2500000 amu. Since there has recently been interest by other researchers in the details of this source, we would like to present some of the main features of our cluster source in Sect. 2 of this contribution.

In order to study large clusters, it is not sufficient to just produce them, they have to also be characterized and detected, usually involving the recording of a mass spectrum. To correctly design a mass spectrometer with a reasonable resolution and a great mass range, the velocity distribution of the clusters in the beam has to be known. Therefore, a description of a cluster source is incomplete without some knowledge of the cluster beam produced. Section 3 will deal with the most important property of the cluster beam, the velocity distribution. We will present the experimental data and qualitatively interpret them using a simple model. A method of doubling the detectable mass range (by using doubly-ionized clusters) will be discussed. We intend this article to be mainly informative to the experimentalist and will therefore limit ourselves to a mainly qualitative discussion of the results.

After guiding large clusters through the spectrometer, they must, of course, be converted into an electrical signal upon arrival at the detector. With increasing cluster mass, this tends to become difficult. Because of the low velocities these clusters posses even at kinetic energies of several thousand eV, the probability of ejecting a secondary electron from the detector (usually a multi-channel plate) on impact is low [6–9]. We will describe our detector setup, the detectability of very large masses, and its dependence on the post-acceleration voltage in Sect. 4.

In our experiments we use photoionization time-of-flight (TOF) mass spectrometry. Figure 1 shows a schematic representation of the experimental setup consisting of three basic components: the cluster condensation cell on the left, a differential pumping stage in the center, and the TOF-mass-spectrometer on the right. Inside the condensation cell, vapor of the selected cluster material is produced by an oven and cooled in an inert-gas atmo-

* *Permanent address:* Central Laboratory of Photoprocesses, Bulgarian Academy of Sciences, 1040 Sofia, Bulgaria

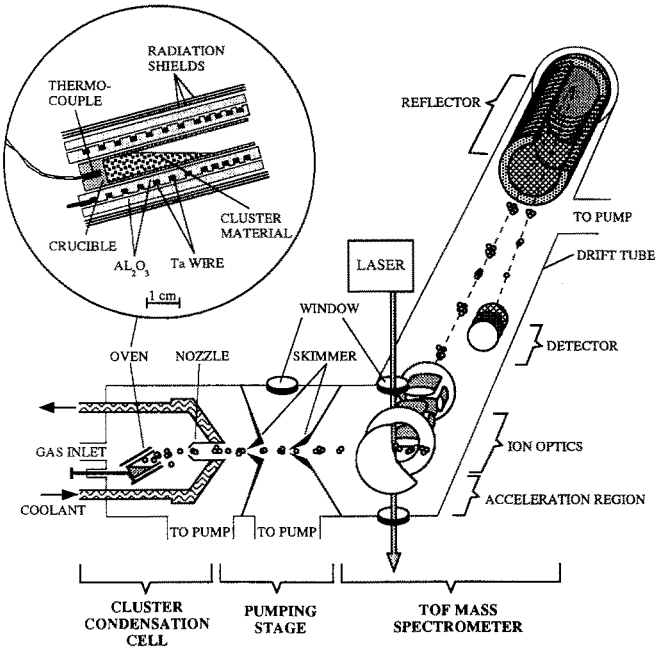

Fig. 1. Experimental arrangement for cluster beam formation and time-of-flight mass analysis. The inset shows a more detailed view of the oven

sphere causing clusters to condense out of the then supersaturated vapor. Together with the flow of inert gas, the clusters thus formed are transported through a nozzle into the differential pumping stage. This unit, consisting of three chambers separated by skimmers, removes the excess inert gas, leaving a collimated cluster beam passing through the acceleration region of the TOF-mass-spectrometer. The clusters are ionized inside the focus of the ion optics and accelerated at right angles into the spectrometer.

The mass spectrometer has a resolution of over 20000. In order to achieve such a high resolution, the axis of the spectrometer has to be oriented at right angles to the neutral cluster beam. Forcing the ions to make a 90° turn in order to enter the spectrometer becomes increasingly difficult for large clusters having high kinetic energies perpendicular to the spectrometer. The maximum kinetic energy that can be compensated for depends on the design of the ion optics of the spectrometer. The greatest mass detectable is thus a function of the velocity of the clusters in the beam. Details of the spectrometer have already been published and will not be repeated here [10–13].

2. The cluster source

In this section, we will focus on the cluster condensation cell, briefly describing its construction (inset of Fig. 1) and demonstrating the influence of different adjustable working parameters on the mass distribution of the clusters produced.

The oven consists of an Al_2O_3-tube with a Ta-wire wrapped around for ohmic heating. This unit is placed inside a second Al_2O_3-tube for thermal isolation. Several layers of Ta-foil on the outside reduce heat losses due to radiation and convection.

A crucible containing the material to be evaporated is placed inside the oven cavity. The oven temperature is measured by a thermocouple touching the bottom of the crucible. By mounting the oven assembly onto a linear motion feedthrough, a continuous variation of the oven-nozzle distance becomes possible. Oven temperatures are typically chosen to result in a vapor pressure of about 0.1 mbar. To produce clusters containing two elements, for example C_{60} covered with alkali metals, two separate ovens, each containing one of the component elements, can be placed inside the oven chamber. Tilting slightly the adjacent openings of the ovens towards each other, the vapor clouds will mix, producing clusters whose stoichiometry can be adjusted by the relative temperatures of the ovens.

The inert gas flow into the chamber can be precisely adjusted with a calibrated needle valve. The gas is cooled by cooling the walls of the chamber (including the nozzle) with liquid nitrogen. Typical gas pressures used range from 1 to 3 mbar. The gas flow through the chamber is around 100 mbar l/min at 90 K, causing an average flow velocity in the wide part of the chamber of approximately 10 m/min.

The nozzle usually used is a tube of 30 mm length and 4.5 mm inside diameter. At the upstream end the nozzle is conical with a sharp-rimmed opening of 3 mm in diameter. This design was found to reduce the build-up of condensed cluster material in the nozzle. Shortening the nozzle increases the gas flow only slightly, suggesting that the main pressure gradient is located at the nozzle openings. The total cluster signal, however, strongly decreases due to a decline in beam collimation in a short nozzle.

When attempting to optimize the cluster yield and distribution with respect to very large clusters, there are four parameters of our cluster source that can be varied: inert gas pressure, oven temperature, inert gas type, and oven-nozzle distance. In the following paragraphs we will characterize the source by presenting the effects each

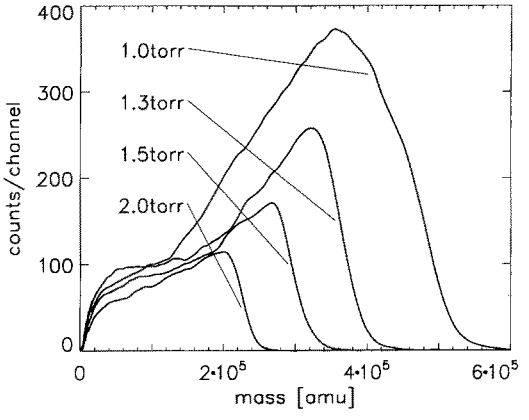

Fig. 2. Mass spectra of Na-clusters produced at different He-pressures in the oven chamber (oven temp.: 570 K). The cutoff on the heavy mass side is caused by the ion optics (see text)

of these parameters has on the cluster distribution. The measured spectra have been smoothed since we are interested in only the general shape of the spectra.

Figure 2 shows mass spectra of Na-clusters recorded at different pressures of the inert gas He (oven temperature 570 K, acceleration voltage of the TOF-spectrometer: 4,2 kV). With increasing He pressure the upper mass limit of the distribution rapidly decreases.

A first interpretation would be that due to changed condensation parameters in the source, very large clusters are no longer formed. This interpretation is, however, not correct. As previously pointed out in Sect. 1, the ion optics guiding the ionized clusters into the spectrometer at right angles will have an upper limit in the kinetic energy it can handle. When increasing the He pressure in the source, the velocity of the clusters and consequently their kinetic energy will increase, shifting the corner-turning cutoff of the ion optics to lower masses. The cutoff in the mass spectra is therefore not related to the real mass distribution, but is an artifact caused by the ion optics. The real distribution of Na-clusters will extend to much greater masses as will be shown in Sect. 3. Obviously, in order to observe very large clusters, the gas pressure in the source has to be kept low. However, which pressure is best to produce very larger clusters cannot be deduced from the data shown in Fig. 2 (and of course, producing very large clusters that you cannot see is rather useless). Note that the acceleration voltage used in the above measurement is the same as in all measurements presented in Sect. 3, leading to comparable conditions for the position of the corner-turning cutoff.

A more feasible method of adjusting the mass distribution is varying the oven temperature. Figure 3 shows Na mass spectra recorded at different oven temperatures (He-pressue: 1 torr, acceleration voltage: 5 kV). The quantity of large clusters produced clearly rises with increasing oven temperature due to the higher vapor pressure and extension of the vapor cloud. On the heavy mass side, the distribution is again limited by the corner-turning cutoff. The difference in the cutoff position for equal pressures in Figs. 2 and 3 is due to the different acceleration voltages (see Sect. 3).

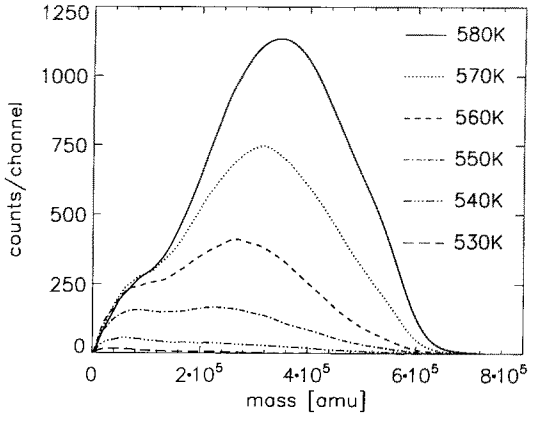

Fig. 3. Mass spectra of Na-clusters produced at different oven temperatures (He pressure: 1 torr)

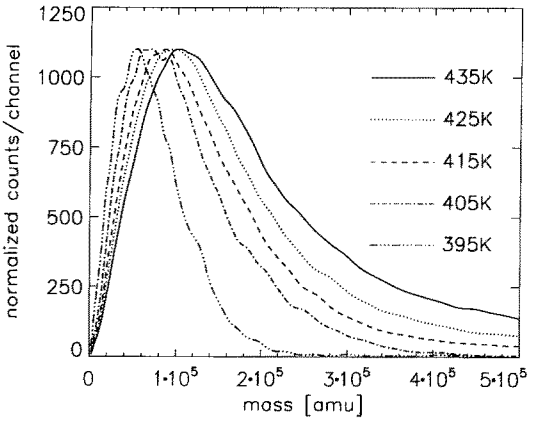

Fig. 4. Mass spectra of Cs-clusters produced at different oven temperatures (He-pressure: 1 torr). The spectra have been normalized to equal maximum heights

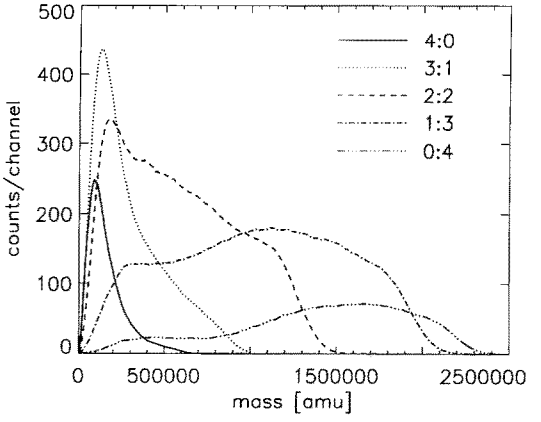

Fig. 5. Mass spectra of Cs-clusters produced at different mixtures of helium and argon in the oven chamber. The spectra are labelled with the ratios of helium to argon partial pressure (total pressure 1 torr. oven temp.: 420 K)

Figure 4 shows the effect of oven temperature on mass spectra of Cs-clusters (He-pressure: 1 torr). The spectra have been normalized to equal maximum heights in order to make the mass shift more evident.

The limitations imposed on the cluster size by the corner-turning cutoff (situated at $7 \cdot 10^5$ amu) are not so severe in the case of Cs-clusters since these do not seem to "like" forming very large clusters in the He atmosphere. This can be greatly altered when using a mixture of helium and argon to quench the vapor. In Fig. 5 mass spectra of Cs-clusters at different He/Ar mixtures are shown. The spectra are labelled with the ratios of He to Ar partial pressure, the total pressure is always 1 torr. The temperature was kept around 420 K.

It is interesting to note that, when increasing the Ar partial pressure, the distribution not only shifts its weight to higher masses (probably due to more efficient cooling of the vapor by the heavier argon), but the corner-turning cutoff also moves to greater masses. This is due to the fact that at equal pressure gradients, the Ar-flow and thus the velocity and kinetic energy of the clusters will be smaller than in the case of He. For pure argon

in the chamber, the main portion of the cluster distribution produced probably lies outside the "mass window" visible to the spectrometer, thus causing the decline in signal. This effect is even more drastic in the case of Na clusters. For the sake of brevity, we will refrain from discussing the effect of other inert gas mixtures.

The last and least effective parameter in producing large clusters is the oven nozzle distance: with increasing the distance from 30 mm to 100 mm the distribution shifts only slightly to higher masses. It seems that the region of cluster formation is smaller than the minimum distance of 30 mm obtainable in our source. More pronounced is the effect of oven-nozzle distance on the total signal: decreasing the distance below approx. 70 mm causes a steep decline in signal. The optimum distance has to be found individually for each cluster material.

3. Velocity distribution

After having presented some details of our cluster source, we will now turn to discussing properties of the cluster beam leaving the source, focussing mainly on the velocity distribution of the clusters.

In order to perform velocity measurements, the clusters were ionized with a pulsed excimer or dye laser beam between the two skimmers of the differential pumping stage. Several hundred μs later, the acceleration field and quadrupol lenses of the TOF-spectrometer were switched on. Only ions having reached the focus of the ion optics at this time will be focussed onto the detector. Scanning the delay between the laser pulse and the switching of the electric fields through the appropriate time range and recording mass spectra at specific delay times, a set of spectra, each associated with a certain velocity, is obtained. From this data, velocity distributions for a specific cluster mass can be extracted. This procedure was performed for clusters of different alkali metals at He pressures ranging from 0.8 torr to 2 torr (below 0.8 torr the cluster intensity becomes too weak, exceeding 2 torr is too much for the pumps). The distance along the cluster beam between the point of ionization and the focus of the ion optics is 200 mm. The width of the laser spot and the focus are both less than 0.5 mm, leading to an uncertainty in the velocity of below 0.5%. The rise time of the acceleration field of approximately 50 ns is negligible as compared to the average delay time of around 500 μs.

Figure 6 shows the measured velocity distributions for different masses of Na-clusters. The height of the curves represents the signal integrated over a mass interval of 1000 amu symmetrical to the mass values denoted on the axis. The relative heights of the maxima of each curve correspond to the detected mass distribution. The He pressure in the source was 0.8 torr, a laser pulse with approx. 0.3 μJ/mm^2 at 193 nm was used for ionization.

There are two different qualities of the cluster beam which can be deduced from the data presented in Fig. 6: First, the velocities of the clusters which we will discuss further along. Secondly, we can obtain more information about the real mass distribution of clusters produced by the source. This aspect will be discussed in the following paragraphs.

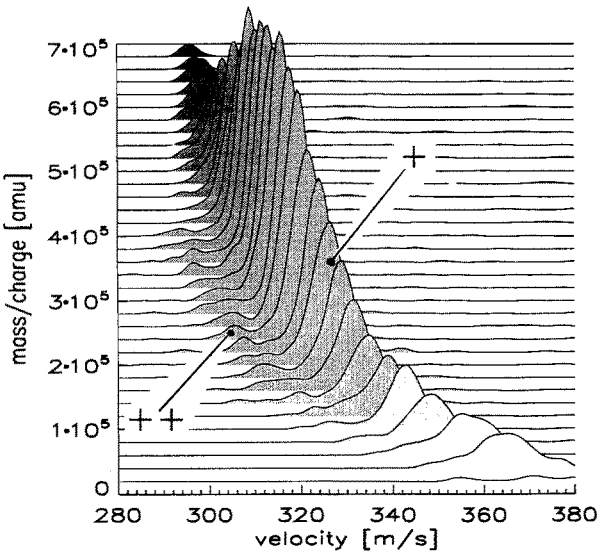

Fig. 6. Velocity distributions for different masses of Na-clusters at a He-pressure of 0.8 torr in the source. A laser pulse with 0.3 μJ/mm^2 at 193 nm was used for ionization. The high 'ridge' corresponds to singly-ionized clusters, the lower one to doubly-ionized clusters

An interesting feature in Fig. 6 is the presence of a second, rather small "ridge" at the left foot of the dominant ridge. The small ridge can be varied in height by changing the intensity of the ionizing laser pulse. This ridge corresponds to the doubly-ionized clusters. Since their actual mass is twice the value recorded by the spectrometer, their velocity distribution is centered at the same value as that of the singly ionized clusters (represented by the large ridge) found at twice their recorded mass. This can be easily verified from Fig. 6.

The maximum in height of both ridges is found to be around 300000 amu (detected, not real mass). Obviously, the mass distribution of the cluster beam implied by the usually observed mass spectra of mostly singly ionized clusters does not reflect the real mass distribution in the neutral cluster beam that, as we find from the doubly-ionized clusters, extends to much larger masses. This becomes more apparent when increasing the intensity of the ionizing laser pulse, as shown in Fig. 7 (1 torr He, 16 μJ/mm^2, 248 nm). The broadening of the peaks is due to evaporation of the clusters caused by the high photon flux and the subsequent heating. The ridge of doubly-ionized clusters becomes very strong. Obviously, the cluster beam produced by our source contains clusters of masses up to 1000000 amu (45000 Na-atoms). The point where the ridges disappear at high masses correspond to preionization kinetic energies of $\simeq$330 eV for the singly ionized, $\simeq$660 eV for the doubly-ionized clusters at an acceleration voltage of 4.2 kV. Varying the acceleration voltage and all potentials of the focussing optics by a fixed factor will vary the cutoff energy by the same factor. Without switching the ion optics, we can raise the acceleration voltage to 5 kV. The cutoff

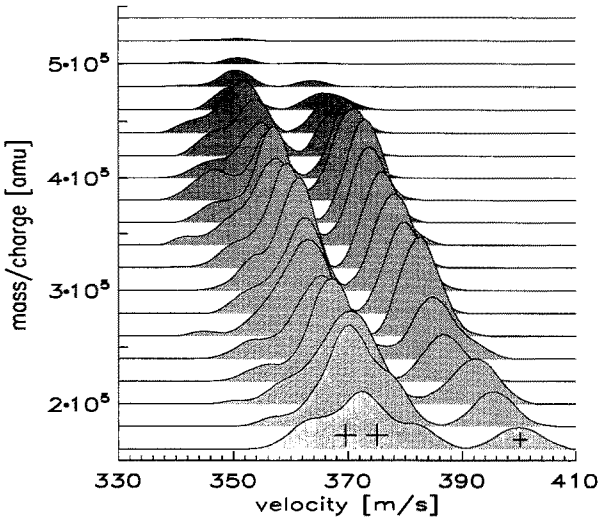

Fig. 7. Velocity distribution of Na-clusters at higher laser fluence than in Fig. 6 (16 μJ/mm², 248 nm; He-pressure: 1 torr). The ridge of doubly-ionized clusters is clearly visible. Broadening of the peaks is due to evaporation of the clusters

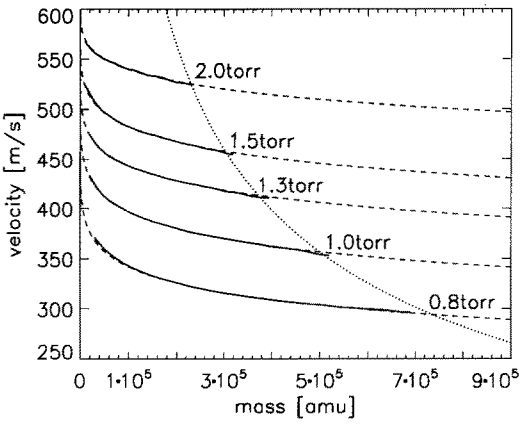

Fig. 8. Mean velocities of singly-ionized Na-clusters at different He-pressures in the source. The *solid lines* represent the measured data, the *dashed lines* are calculated from the model described in the text. The *dotted line* corresponds to a kinetic energy of 330 eV

energy then becomes approx. 390 eV for singly ionized clusters. Clearly, the high mass limit detectable with the spectrometer is, in this case, not set by the cluster source but by the energy cutoff of the ion optics (note that the cutoff depends on the ratio of mass-to-charge as expected of electric fields). For low He pressures where the cutoff shifts to higher masses, the detector will also limit the mass range (see Sect. 4).

The clear separation in velocity or arrival time for the singly and doubly-ionized clusters visible in Fig. 7 opens an interesting possibility to extend the mass range of the experiment by a factor of two (if the spectrometer does not have the resolution to identify every other doubly-ionized cluster directly in the mass spectrum): ionizing with sufficiently high intensity some distance upstream of the focus of the ion optics and the switching on of the fields with a fixed delay, the mass spectrum will show two clearly separated ion distributions, one corresponding to the singly-ionized, one to the doubly-ionized clusters. If the positions of these two distributions at different delay times have been obtained from an experiment as presented above, the signal due to the singly-ionized clusters can be easily discriminated by the data acquisition program. Continuously varying the delay time while accumulating the mass spectra will lead to a spectrum containing only doubly-ionized clusters with twice the mass range possible by just taking the singly-ionized clusters. Experiments can be performed with this extended mass range, as long as they do not cause an overlap of the two 'ridges'. Of course, laser wavelength and intensity have to be chosen carefully to avoid triply-ionized clusters.

The mean velocities as a function of cluster mass for different He pressures are shown in Fig. 8 for singly-ionized Na clusters. The solid lines represent the measured data, the dashed lines are fits obtained from a model described below. The dotted line corresponds to the ion optics cutoff at a kinetic energy of 330 eV. At every He pressure, the detected mass distributions cut off almost exactly at this point, as expected. Below approximately 20000 amu (1000 Na atoms) the cluster intensity produced by our source is too small to observe. The decrease in velocity with increasing mass, commonly termed "velocity slip" in the literature [14–16], can be easily understood: the heavy metal clusters, having almost zero velocity and very small density inside the oven chamber of the source, can be thought of as being swept through the nozzle into the vacuum by the He flow. Acceleration of the clusters is achieved by collisions with the fast flowing He gas. Assuming rigid sphere collisions, the cross section of a cluster increases with the square while its weight increases with the cube of its radius. Consequently, the smaller clusters will be accelerated more quickly. After passing through an acceleration distance in the range of the nozzle length, the lighter clusters will have gained a higher velocity. Extrapolating the cluster mass to that of He should yield the average He velocity. It is, however, not possible to reasonably perform such an extrapolation from the data in Fig. 8. Direct measurement of the He velocity by placing a very light ion in the He flow is, unfortunately, not possible in our experiment, since such a particle would have a kinetic energy of only a few meV and can thus be easily prevented from entering the ion optics by stray charges present on the insulators of the ion optics.

Measuring curves as shown in Fig. 8, the researcher is, of course, challenged to go beyond a merely verbal interpretation. So, in order to at least qualitatively describe the form of the curves shown in Fig. 5 and obtain some notion of the He velocity, we propose the simple model developed in the following paragraphs (more elaborate models describing the velocity slip have been presented in the literature [17, 18], but as we will see below, our simple model is sufficient to interpret the data). We should mention at this point that our cluster source was designed to produce intense beams of large clusters and not intended to be an easily studied model of gas flow characteristics. Therefore, we cannot give an exact treat-

ment but only lay a basis for qualitative understanding of the beam properties.

Let us assume the clusters and the helium as being rigid spheres, the helium flowing with a constant density n and average velocity v_{He} through the nozzle. Having the main pressure gradients at the ends of the nozzle (see Sect. 2), this assumption might not be altogether faulty. Averaging over the collision parameter, elastic collisions between the He atoms and the clusters will increase the cluster momentum in direction of the flow by $\mu\cdot(v_{He}-v_c)$, where μ is the reduced mass of the collision partners and v_c the cluster velocity. Components of momentum transfer to the clusters perpendicular to the direction of flow are assumed to average out after many collisions or otherwise cause the cluster to diverge from the beam. The collision rate is $n\cdot\sigma\cdot(v_{He}-v_c)$, where σ is the total collision cross section. The time derivative of the cluster momentum (mass M) will then be given by

$$M\dot{v}_c(t)=\mu n\sigma(v_{He}-v_c(t))^2. \tag{1}$$

The solution for $v_c(t)$ becomes

$$v_c(t)=v_{He}-\left(\frac{\mu n\sigma t}{M}+\frac{1}{v_{He}}\right)^{-1}, \tag{2}$$

satisfying the boundary conditions

$$v_c(0)=0, \qquad v_c(t\to\infty)\to v_{He} \tag{3}$$

Replacing σ by $\pi(3M/4\pi\rho)^{2/3}$ where ρ is the mass density of the cluster material and neglecting the He mass m_{He} in the denominator of μ, we find an implicit equation for v_c as a function of the acceleration length x:

$$M=\frac{9\pi}{16}\frac{(m_{He}\cdot n\cdot x)^3}{\rho^2}\left[\frac{v_c}{v_{He}-v_c}-\ln\left(\frac{v_c}{v_{He}-v_c}+1\right)\right]^{-3}. \tag{4}$$

For the acceleration length x we take the length of the nozzle (8 mm downstream is the first skimmer where, at the latest, the flow will be molecular and the collision rate neglectable). Errors in x can be projected into n. Since we have no possibility to determine the average He velocity v_{He} and density n from the experiment, we will use them as adjustable parameters to fit our model to the measured data using the implicit equation above. These fits are represented by the dashed lines in Fig. 8.

Table 1. Velocity and density of the He flow through the nozzle at different He pressures inside the cluster source. The values are obtained by fitting our model (see text) to the experimental data shown in Fig. 8

Source	v_{He}[m/s]	$n[10^{20}\,\mathrm{m}^{-3}]$
0.8 torr	480	276
1.0 torr	527	369
1.3 torr	549	574
1.5 torr	581	702
2.0 torr	607	1312

Obviously, the model can be made to fit quite nicely by adjusting v_{He} and n. These values are listed in Table 1.

At this point, we should look at the width of the measured velocity distributions. Almost independent of cluster mass and He pressure, we find the width (FWHM) of the velocity distributions to be less than 5% of the mean velocity. This small width may seem surprising at first, however, calculating the translational temperature corresponding to the measured widths of the heavy clusters, we find values of approx. 300 K. Considering the temperature of the helium of below 100 K, we should rather look for a reason why the peaks are so broad. A likely cause of this broadening is a radial variance of the mean flow velocity of the He gas: the Reynolds number of the He flow through the nozzle has a value of less than 100 for all He pressures. The flow can be expected to be laminar and thus have a radially decreasing mean flow velocity. Since the limiting aperture of the beam collimating system has an effective diameter of 1.5 mm (one-third of the nozzle diameter) at the point of ionization, a finite portion of the radial velocity profile will be transmitted. Consequently, the measured velocity distribution will be broadened by a superposition of distributions originating from different parts of the cluster beam. The above argument can be verified by decreasing the width of the ionizing laser spot to 0.1 mm perpendicular to the cluster beam and scanning it across the beam: the velocity distributions decrease slightly in width and the centers of the distributions vary by approx. 1%. A further decrease of the relative width of the velocity distributions, for example by decreasing the He temperature, raising the mean flow velocity, etc., would lead to a very interesting application: due to the mass-dependent velocity of the clusters, a mass selection of neutral clusters, e.g. for deposition as thin films, could be accomplished by using a mechanical chopper to perform a velocity selection [17, 19]. With the width of the distribution we presently observe, the mass resolution is around 4. By decreasing the relative width, a higher resolution should be possible.

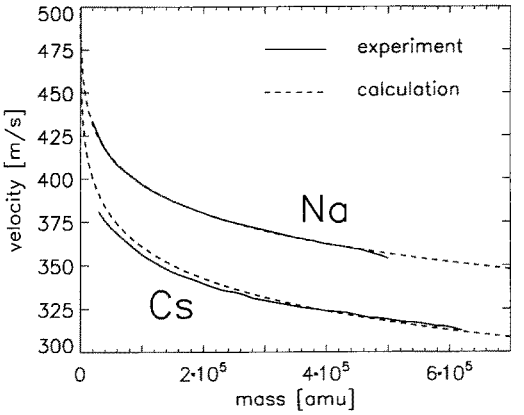

Fig. 9. Mean velocities of singly-ionized Na- and Cs-clusters at equal He-pressure (1 torr). The *solid lines* represent the measured data, the *dashed lines* are calculated from the model using a He-velocity of 527 m/s and a He-density of $3.69\cdot10^{22}\,\mathrm{m}^{-3}$ for both curves

Measuring the velocities of clusters having a mass density higher than that of Na, e.g., Cs, lower velocities and greater cutoff masses are found at equal He pressures. This fact can be easily understood from the simple hard sphere collision picture: comparing a Cs and a Na cluster of equal mass, the Cs cluster will have a smaller collision cross section, thus experiencing less acceleration by the He flow. Figure 9 compares the mass-dependent velocities of Cs and Na clusters at a He pressure of 1 torr. The dashed lines are obtained from (4) using values for v_{He} and n listed in the table above (1 torr) in both curves and the bulk densities of Cs and Na. Obviously, the dependence of the cluster velocities on the mass density is correctly predicted by our model. For the sake of brevity, we will refrain from presenting velocity measurements using different nozzles and inert gases.

4. Detector

Last, but not least, a spectrometer requires a detector to count the incident ions. In our experiment, the detector consists of two multi-channel plates (MCP) in series. The incoming ions experience a maximum post-acceleration voltage of 10.6 kV before reaching the MCP. Across each MCP there is a potential of 1 kV. The electrons which are emitted from the rear MCP are accelerated by an additional 8 kV onto a collector plate, producing a current pulse which is sent as one count to the data acquisition electronics.

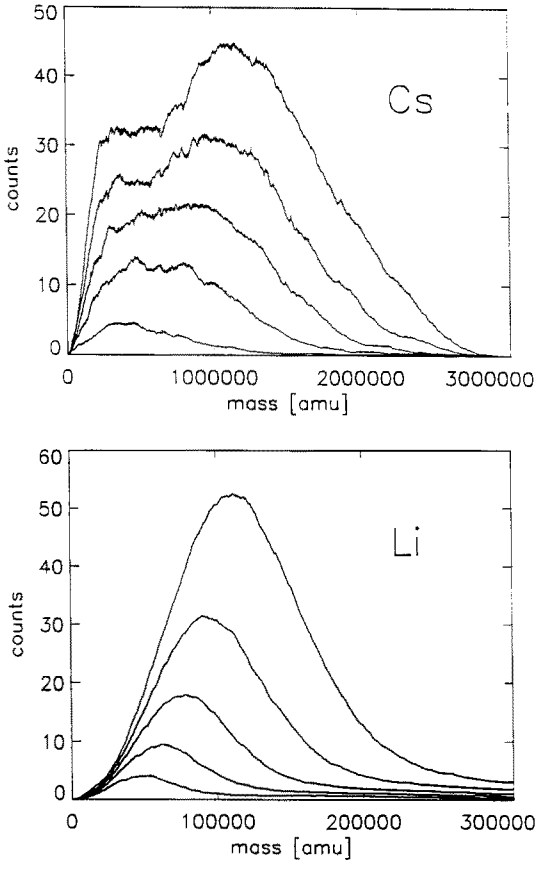

Fig. 10. Mass spectra of cesium and lithium clusters for various acceleration voltages (8, 10, 12, 14, 16 kV). With maximum post-acceleration cesium clusters can be detected up to 3 million amu while for lithium the upper limit is 300000 amu

It has been reported that the yield of secondary electrons emitted from a target by the impact of an ion decreases with decreasing ion velocity down to a threshold velocity below which the emission of secondary electrons no longer takes place. In the literature this threshold velocity is found to be around $2 \cdot 10^4$ m/s, depending slightly on the ion material and the surface of the target [6–9].

We could not confirm this in our experiments. Since all cluster ions are accelerated to equal energies, large clusters are much slower than small clusters when they arrive at the detector. The threshold velocity of $2 \cdot 10^4$ m/s corresponds to an upper detectability limit of about 8000 amu, which is much less than the several million amu clusters we have observed.

Nevertheless, in our experiments the detected cluster signal strongly depends on the cluster energy. This can clearly be seen in Fig. 10 where mass distributions of cesium and lithium clusters have been measured for various acceleration voltages. We changed only the post-acceleration to be sure not to influence the transmission of the ion optics, the focussing conditions, or the size of the ionization volume. With maximum post-acceleration voltage cesium clusters can be detected up to nearly 3 million amu while for lithium the upper limit is 300000 amu. For small cluster (up to 5000 atoms) the signal seems to decrease linearily with the acceleration voltage while for large clusters the detection probability dramatically changes if the voltage is slightly varied. Cesium clusters with a energy of 8 keV can hardly be detected if their size is larger than 1500000 amu, for lithium this threshold is 150000 amu.

To discuss the features of Fig. 10 in more detail, it is useful to describe the detected cluster signal in terms of a 4-factor formula:

$$I(n, U_{acc}, U_{post}) = D(n) \cdot f_{ion}(n) \cdot f_{foc}(U_{acc}, n) \cdot f_{det}(U_{acc} + U_{post}, n) \quad (5)$$

n denotes the number of atoms, U_{acc} the acceleration voltage and U_{post} the post-acceleration voltage. The first term in Eq. (5), $D(n)$, describes the cluster distribution produced by the oven. The last three factors are all probabilities and smaller than 1. The second term, f_{ion}, gives the ionization probability which, of course, is also dependent on the intensity and wavelength of the ionization laser. f_{foc} describes the transmission of all apparatus dependent parameters as the ion optics or the reflectron. The detection probability is given by f_{det}. In Eq. (5) we have assumed that the detection probability is a function of the total energy and the number of atoms in the clusters.

In Fig. 10 the detector signal is plotted for various values of the parameter U_{post}. The ratio between these curves should give a precise description of the detection probability. For example:

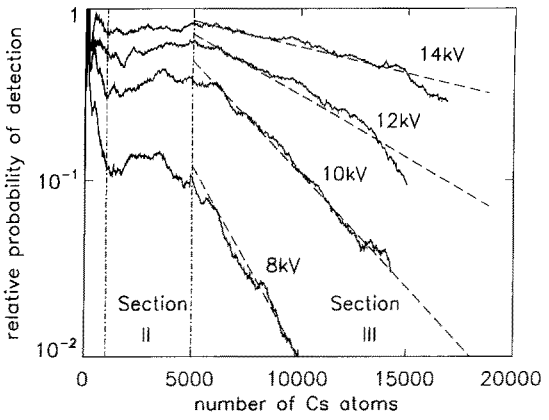

Fig. 11. The relative probability of detection for cesium clusters. The signal has been normalized to the signal of maximum accelerations voltage (16 kV). The size range can be divided into three section: A saturation regime (section I), a regime of constant relative detection probability (section II), and a regime of exponential decay (section III). The interpolating lines in section III have a slope of $-8\ \mathrm{eV}/E_{\mathrm{atom}}$

$$\frac{I(n, U_{\mathrm{acc}}, 8\mathrm{kV})}{I(n, U_{\mathrm{acc}}, 4\mathrm{kV})} = \frac{f_{\mathrm{det}}(16\mathrm{kV}, n)}{f_{\mathrm{det}}(12\mathrm{kV}, n)} \tag{6}$$

In Fig. 11 this relation is plotted logarithmically for cesium clusters. Three different size ranges can be distinguished. For small clusters the lines converge to one. This is the saturation regime (Sect. I) where all clusters are detected independent of their energy.

Between 1000 and 5000 cesium atoms (Sect. II) the ratio of the cluster signals is nearly independent of their mass. It only depends on the voltage but not on the cluster size. In that size range the detection probability can be described by the product of a mass and a energy dependent factor:

$$f_{\mathrm{det}}(n, U) = f_1(n) \cdot f_2(U) \tag{7}$$

A decrease of the total energy from 16 keV to 8 keV reduces the signal by a factor of approximately 10.

For large clusters with more than 5000 atoms (Sect. III) the situation is different. In that size range the signal is more sensitive to the acceleration voltage. On the logarithmic scale the signal decreases linearly with increasing cluster size. The ansatz

$$f_{\mathrm{det}} \simeq f_3(E) \cdot f_4(n) \cdot \exp\left(-\frac{\Delta E}{E_{\mathrm{atom}}}\right) \tag{8}$$

is a good fit to the data. The function $f_3(E)$ is an energy-dependent constant. $f_4(n)$ is a factor which only depends on the number of atoms and not on the energy of the clusters. It cannot be evaluated with the method discussed here. E_{atom} describes the total energy per sodium atom ($E_{\mathrm{atom}} = U \cdot e/n$) and ΔE is a constant activation energy which is found to be 8 eV for all materials (Cs, Na, and Li). Apparently, this activational energy is comparable to the chemical binding energy or the work function of metals. The third term in (8) is responsible for the exponential decay of the signal with cluster size. If, as predicted by (8), the detected cluster signal is a function of the kinetic energy per atom, on an atomic scale the onset of the exponential decay should not depend on the cluster material. This was observed for lithium and sodium clusters. The relative logarithmic intensities of lithium and sodium spectra are plotted in Fig. 12. The x-axis is the number of atoms. Although the masses of lithium, sodium, and cesium differ by a factor of about 20, the normalized spectra of Figs. 11 and 12 are very similar. The detectability of large clusters obviously is a function of the energy per atom and not only of the total energy or velocity of the clusters. For all materials the slope of the lines in section III can be approximated by $-8\,\mathrm{eV}/E_{\mathrm{atom}}$. The onset of the exponential decay starts for all materials in the range between 5000 and 8000 atoms. For this reason we are able to observe cesium clusters with masses far above 2 million amu, lithium clusters, however, only up to 300000 amu.

Since the signal for large clusters decays exponentially with the energy per atom, the signal in that size range is very sensitive to changes in the acceleration (or post-acceleration) voltage. This is demonstrated very clearly in the lithium spectra of Fig. 10. As predicted by (8) the detectability threshold increases with the acceleration voltage.

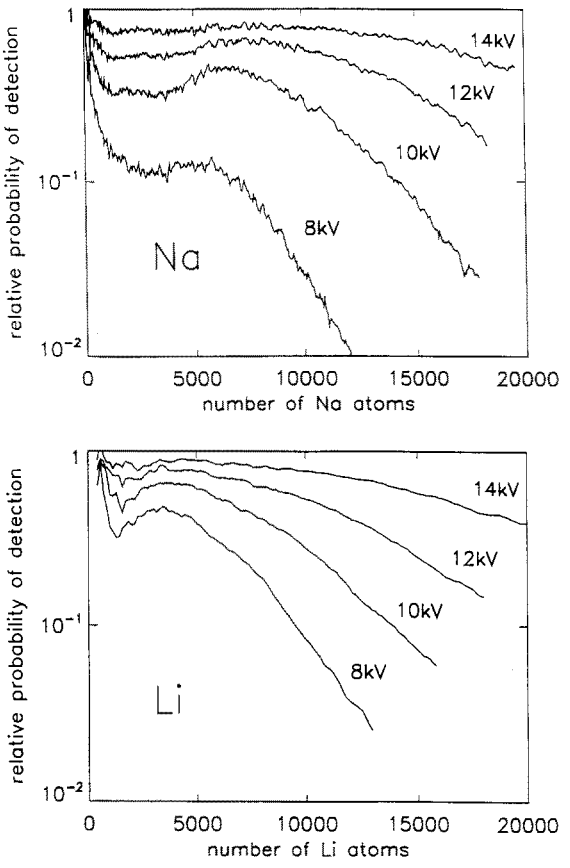

Fig. 12. The relative probability of detection for sodium and lithium clusters. Although the masses of sodium, lithium, and cesium atoms differ by a factor of 20, the relative probability of detection is very similar when plotted as a function of the number of atoms

It should be mentioned here that the f_{det} may include an effect peculiar to our instrument. Before the clusters arrive at the detector they are post-accelerated and have to pass a fine grid. Large clusters might break apart when they hit the grid. In that case, the charged fragments are accelerated to the surface of the channel plate. Since they are much smaller than the initial clusters, they arrive at much higher velocities at the detector which increases their detection probability. However, such a process should also spoil the resolution of the mass spectrometer. At least in the size range where single peaks in the spectrum can be distinguished (for cesium clusters up to several 100000 amu) we have not observed such an effect.

In conclusion, the described channel-plate detector is able to detect very large clusters up to several million mass units, much larger than predicted by theory. There is evidence that the detectability of these 'small particles' depends on the energy per atom. Above ~ 6000 atoms the cluster signal exponentially decays with the cluster size. This behaviour was found for various alkali metals. Clusters having an energy even less than 1 eV/atom could be detected.

5. Conclusions

In this contribution we have presented some details of our cluster source and discussed the influences of several variable parameters on the cluster distribution produced.

The highest yield of very large clusters was obtained at high oven temperatures, with heavy inert gases used for the quenching of the vapor. Inert gas pressure has to be kept low in order to shift the corner-turning cutoff to larger masses. The data presented here show that the source can produce clusters with more than 45000 atoms in the case of Na and 2500000 amu in the case of Cs. We hope this information to be of service to other research groups wishing to produce similar beams with very large clusters. Measurements of the velocity distributions of the clusters in the beam at different inert gas pressures were discussed, demonstrating the presence of a corner-turning cutoff at a kinetic energy characteristic of the ion optics. The observed mass-dependent velocity slip between clusters and inert gas atoms in the beam was interpreted using a simple, rigid sphere-collision model for the acceleration process of the clusters. The relative widths of the velocity distribution were found to be below 5% (FWHM).

Regarding the detector, we demonstrated that even though the large clusters are significantly slower upon arrival at the detector than the threshold velocity stated in the literature, they nevertheless produce a detectable signal. The influence of the post-acceleration voltage onto the greatest mass detectable was discussed.

We gratefully acknowledge the expert technical assistance of H. Schaber and stimulating discussions with O.F. Hagena.

References

1. Proceed. 6th Int. Meeting on Small Particles and Inorganic Clusters, Chicago, 1992; Z. Phys. D **26** (1993)
2. Martin, T.P., Näher, U., Bergmann, T., Göhlich, H., Lange, T.: Chem. Phys. Lett. **183**, 119 (1991)
3. Martin, T.P., Bergmann, T., Göhlich, H., Lange, T.: J. Phys. Chem. **95**, 6421 (1991)
4. Martin, T.P., Bergmann, T., Göhlich, H., Lange, T.: Z. Phys. D **19**, 25 (1991)
5. Göhlich, H., Lange, T., Bergmann, T., Martin, T.P.: Mod. Phys. Lett. **B5**, 101 (1991)
6. Baragiola, R.A.: Surf. Sci. **90**, 240 (1979)
7. Alonso, E.V.: Phys. Rev. B **22**, 80 (1980)
8. Thum, F., Hofer, W.O.: Surf. Sci. **90**, 331 (1979)
9. Beuhler, R., Friedman, L.: Chem. Rev. **86**, 521 (1986)
10. Bergmann, T., Martin, T.P., Schaber, H.: Rev. Sci. Instrum. **60**, 347 (1989)
11. Bergmann, T., Martin, T.P., Schaber, H.: Rev. Sci. Instrum. **60**, 762 (1989)
12. Bergmann, T., Göhlich, H., Martin, T.P., Schaber, H., Malegiannakis, G.: Rev. Sci. Instrum. **61**, 2585 (1990)
13. Bergmann, T., Martin, T.P., Schaber, H.: Rev. Sci. Instrum. **61**, 2592 (1990)
14. Cattolica, R., Talbot, L., Coe, D.: In: 10th Int. Symp. on Rarefied Gas Dynamics, p. 161, Leith Potter, J. (ed.). London: Pergamon Press 1977
15. Nanbu, K.: Phys. Fluids **22**, 998 (1979)
16. Raghuraman, P., Davidovits, P.: Phys. Fluids **21**, 1485 (1978)
17. Schwartz, M.H., Andres, R.P.: In: 10th Int. Symp. on Rarefied Gas Dynamics, p. 135, Leith Potter, J. (ed.). London: Pergamon Press 1977
18. Miller, D.R., Andres, R.P.: Proceed. 6th Int. Sympos. on Rarefied Gas Dynamics, Vol. II, pp. 1385, Trilling, L., Wachman, H.V. (eds.). New York: Academic Press 1969
19. Anderson, J.B., Davidovits, P.: Science **187**, 642 (1975)